SANDIA REPORT

SAND2017-5378
Unlimited Release
Printed May 2017

Antenna Loading Impact on the Coupling Response of a Slotted Cylindrical Cavity

Salvatore Campione, Larry K. Warne, Lorena I. Basilio, Rebecca S. Coats, and Roy E. Jorgenson

Prepared by
Sandia National Laboratories
Albuquerque, New Mexico 87185 and Livermore, California 94550

Sandia National Laboratories is a multimission laboratory managed and operated by National Technology and Engineering Solutions of Sandia, LLC., a wholly owned subsidiary of Honeywell International, Inc., for the U.S. Department of Energy's National Nuclear Security Administration under contract DE-NA-0003525.

Issued by Sandia National Laboratories, operated for the United States Department of Energy by Sandia Corporation.

Available to DOE and DOE contractors from
U.S. Department of Energy
Office of Scientific and Technical Information
P.O. Box 62
Oak Ridge, TN 37831

Telephone: (865) 576-8401
Facsimile: (865) 576-5728
E-Mail: reports@osti.gov
Online ordering: http://www.osti.gov/scitech

Available to the public from
U.S. Department of Commerce
National Technical Information Service
5301 Shawnee Rd
Alexandria, VA 22312

Telephone: (800) 553-6847
Facsimile: (703) 605-6900
E-Mail: orders@ntis.gov
Online order: http://www.ntis.gov/search

SAND2017-5378
Unlimited Release
Printed May 2017

Antenna Loading Impact on the Coupling Response of a Slotted Cylindrical Cavity

Salvatore Campione, Larry K. Warne, Lorena I. Basilio, Rebecca S. Coats, and Roy E. Jorgenson
Electromagnetic Theory Department
Sandia National Laboratories
P.O. Box 5800
Albuquerque, New Mexico 87185-1152

Abstract

This report details the effect of antenna loading on the interior near-field response of a resonating cylindrical cavity characterized by a leaky aperture. We find a large field variation within the cavity when a long antenna is introduced within the interior and the antenna load is varied from 0 to 50 Ohms. We also find the effect of absorption losses to be negligible. In order to accurately characterize the coupling into the cavity, a "non-perturbing" sensor (such as a monopole) is recommended. With this approach, the interior field distribution and peak levels characterizing the cavity will be fairly well preserved. In addition to studying the impact of antenna loading on the interior near-field response, the resonant frequencies for the cylindrical structure perturbed by a subwavelength aperture are found to be well estimated by analytical computations.

Intentionally Left Blank

CONTENTS

FIGURES

Intentionally Left Blank

1. INTRODUCTION

The purpose of this report is to explore the interior field response when a resonating cylindrical cavity containing a small perturbing slot (or aperture) is excited by an external electric field. While a simple canonical structure (cylinder with a single rectangular slot) is used for demonstration purposes in this report, the conclusions presented here would apply to more complex cavity structures containing coupling pathways such as small antenna windows, vents, or mechanical joints (forming seams or thin slots). Using simulation results to illustrate near-field effects, the main goal is to show that different interior loading conditions result in very different electric fields within the cavity, even sometimes larger than the incoming field coupled through the aperture inside the cavity. This behavior has also been observed in published literature [1-5].

2. PLANE WAVE EXCITATION OF AN EMPTY CYLINDRICAL CAVITY CONTAININGA SMALL LEAKY APERTURE

We first investigate an empty, perfect electric conductor (PEC) cylindrical cavity with a 0.1" x 6" aperture on one side of the container and positioned at mid-height along the axis of the cylinder. The cylinder has height $h = 1.971$ m and radius $a = 0.4572$ m; a schematic is shown in Figure 1. We compare three simulation results: EIGER (an SNL Method-of-Moments (MoM) code developed under the Advanced Simulation and Computing (ASC) Program [6-8]), FEKO (MoM-based commercial software) [9], CST Microwave Studio (finite-integration-based commercial software) [10]. These dimensions are chosen so that resonant frequencies are in the MHz range where it is numerically easier to match results. Furthermore, we avoid cavity over-moding and reduce the computational time, which would dramatically increase when performing high-frequency responses.

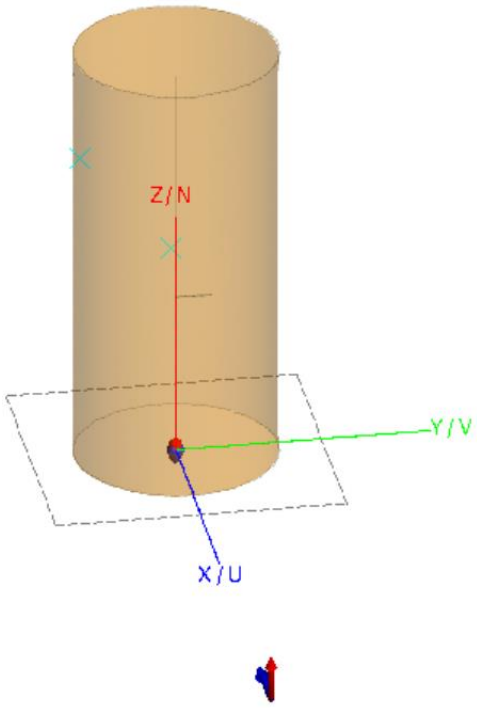

Figure 1. Schematic of a cylindrical cavity with a small 0.1" x 6" aperture being excited by a plane-wave incident field.

We illuminate such a cavity with a plane wave with electric field polarized along the axis of the cylinder as shown in Figure 1. We impose the incident electric field strength to be 1 V/m, so that field quantities greater than 0 dB shown in the figures below represent field enhancements. In *Appendix A* we report the analytical formulation for computing the resonant frequencies for *E* and *H* modes supported by a fully-enclosed cylindrical cavity. Since the small aperture considered in this analysis should only slightly perturb the resonant conditions of the solid cylinder, we will use these formulas to estimate the frequency location of the interior-supported

modes. In particular, we select the lowest order *E* mode (0,1,0) (using equation A21 in Appendix A) and find

$$f_{0,1,0} = \frac{c}{2\pi}\sqrt{\left(j_{0,1}/a\right)^2 + \left(0\pi/h\right)^2} = \frac{3\times10^8}{2\pi}\sqrt{\left(2.40482/0.4572\right)^2} = 251.14\,\mathrm{MHz} \quad (1)$$

We also select a higher order *E* mode (0,1,6) and find

$$f_{0,1,6} = \frac{c}{2\pi}\sqrt{\left(j_{0,1}/a\right)^2 + \left(6\pi/h\right)^2} = \frac{3\times10^8}{2\pi}\sqrt{\left(2.40482/0.4572\right)^2 + \left(6\pi/1.971\right)^2} = 521.13\,\mathrm{MHz} \quad (2)$$

It will be shown later that it is also important to compute the frequency of an *H* mode (1,1,2) (using equation A12 in Appendix A) and of an *E* mode (2,1,0) (using equation A21 in Appendix A) and find

$$f_{1,1,2} = \frac{c}{2\pi}\sqrt{\left(j'_{1,1}/a\right)^2 + \left(2\pi/h\right)^2} = \frac{3\times10^8}{2\pi}\sqrt{\left(1.84118/0.4572\right)^2 + \left(2\pi/1.971\right)^2} = 245.23\,\mathrm{MHz} \quad (3)$$

$$f_{2,1,0} = \frac{c}{2\pi}\sqrt{\left(j_{0,1}/a\right)^2 + \left(0\pi/h\right)^2} = \frac{3\times10^8}{2\pi}\sqrt{\left(5.13562/0.4572\right)^2} = 536.33\,\mathrm{MHz} \quad (4)$$

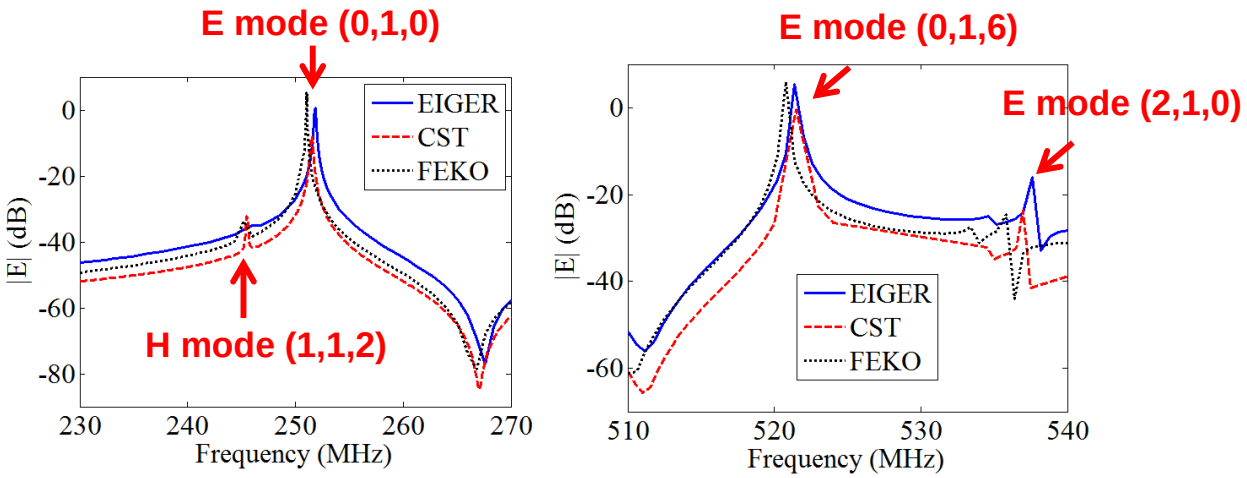

Figure 2. Frequency sweeps performed using EIGER, FEKO, and CST Microwave Studio for the structure in Figure 1. The field is sampled at (*x*, *y*, *z*) = (0, -0.0254, 1) m.

Next, performing two frequency sweeps in the numerical simulations, one between 230 and 270 MHz, the other one between 510 and 540 MHz, we can confirm the resonant frequency locations estimated using the analytical model in Appendix A and, at the same time, verify the agreement among different full-wave solvers (EIGER, CST, and FEKO). These ranges were chosen around the resonance frequencies predicted by Eqs. (1-4). The results are shown in Figure 2(a) for the lowest order *E* mode in Eq. (1), and in Figure 2(b) for the higher order *E* mode in Eq. (2). The observed resonance frequencies appear at the expected values predicted by analytic theory, and a

good agreement is observed when comparing the various full-wave software packages (for example, for the lowest order *E* mode we observe 0.26% error for EIGER, 0.18% for CST, and 0.056% for FEKO). In Figure 2(a), we also observe the presence of the *H* mode in Eq. (3), and in Figure 2(b) we also observe the presence of the *E* mode in Eq. (4).

Below, we also report in Figure 3 a comparison between measurement data (performed both in the anechoic chamber and the mode stirred chamber, see [11]) and EIGER simulations for a cylinder with height $h = 0.6096\,\mathrm{m}$ and radius $a = 0.1016\,\mathrm{m}$, with a 0.02" x 2" aperture on one side of the cylinder, once again located midway along the cylinder length. We concentrate on the lowest order *E* mode (0,1,0) (using equation A21 in Appendix A) and find $f_{0,1,0} = 1.13\,\mathrm{GHz}$. We observe good agreement between measurements and simulations as shown in Figure 3. While the resonance frequency estimated by EIGER agrees well with the two experiments, the amplitudes are somewhat different. In simulation, we were able to have a fine frequency grid around the high-quality resonance, whereas the experiment was limited to a coarse frequency sampling which did not allow us to fully capture the narrow, high quality-factor resonance. A more complete analysis can be found in [11].

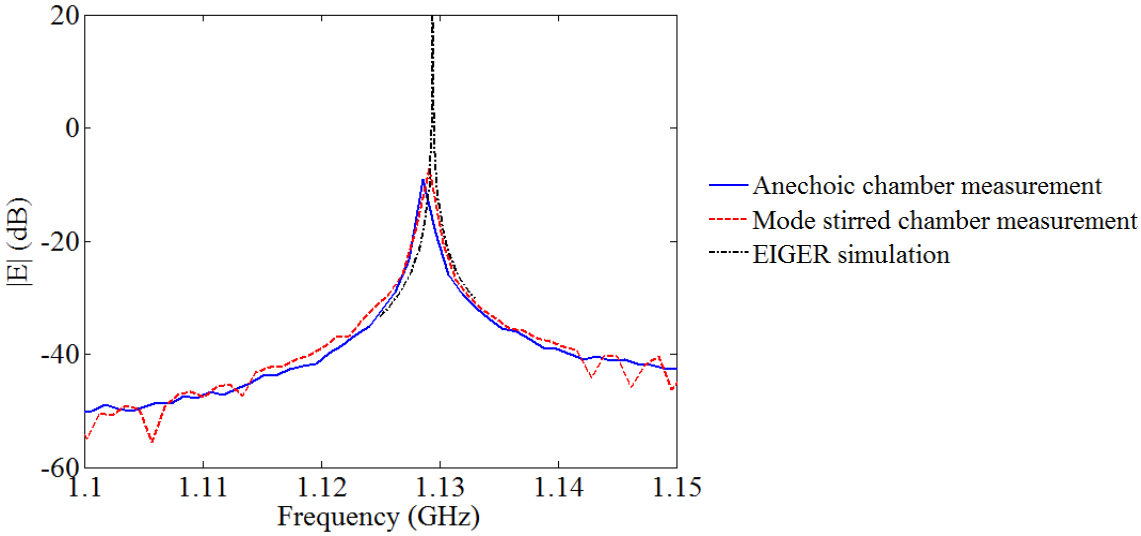

Figure 3. Comparison between experiments and EIGER simulations for a cylinder with a slot as discussed in [11].

3. ANTENNA-LOADED CYLINDRICAL CAVITY WITH A SMALL APERTURE UNDER PLANE WAVE INCIDENCE

We now introduce a long perfect-electric-conductor (PEC) wire antenna at the center of the container, running from the bottom edge (where it is connected through a resistive load that we will be varying from 0 to 50 Ohms) to a height $l = 1.5\,\mathrm{m}$, where it is left open circuited. By varying the antenna loading conditions, we are interested in observing the corresponding effects on the interior cavity field distribution and thereby forming a preliminary basis for experimental best practices when characterizing electromagnetic coupling for complex (leaky) cavities (forexample, when experimentally quantifying shielding effectiveness [11, 12]). In addition to exploring loading effects on the interior near-field magnitudes, we also want to mention that the introduction of the long wire antenna creates new modes. For a long antenna, the resonance is achieved when

$$l = \frac{\lambda}{4} \rightarrow \lambda = 4l = 6\,\mathrm{m} \rightarrow f = 50\,\mathrm{MHz} \tag{5}$$

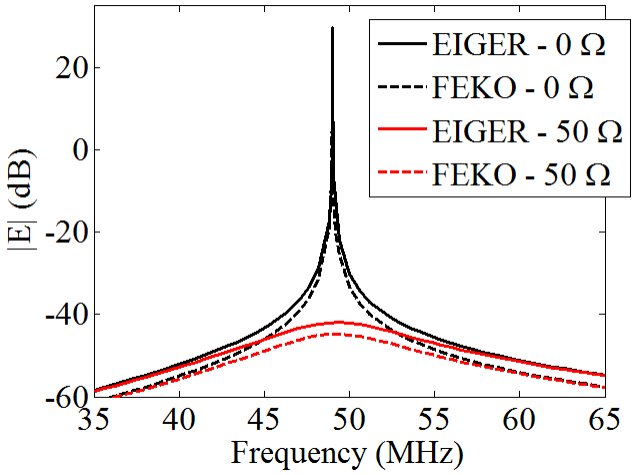

Figure 4. Frequency sweeps performed using EIGER and FEKO for the structure in Figure 1 with a long-wire antenna. The field is sampled at (*x*, *y*, *z*) = (0, -0.0254, 1) m.

Using the full-wave simulator EIGER, we perform a frequency sweep between 35 and 65 MHz with both antenna loading conditions described above. The result is shown in Figure 4, where the frequency range was chosen to well resolve the resonance frequency at 50 MHz as predicted by Eq. (5). One can observe a wide field variation (greater than 60 dB) produced by the presence of the 50 Ohm load when comparing the two conditions. This result demonstrates that in the case of the perturbing antenna loaded by 50 Ohm, the field excited within the cylinder (driven by the exterior electric field) is significantly damped relative to the short-circuited antenna. Thus, if the goal was to experimentally characterize how effective the slotted cylinder was at "shielding" from the exterior field, a 50 Ohm-loaded wire antenna would indicate that coupling into the interior is significantly lower than it is in actuality (as shown when a 0 Ohm loaded antenna had been used). The 50 Ohm loaded antenna perturbs the cavity under measurement by damping

(lowering) the interior field and one would conclude that the slotted cylinder is a better electromagnetic shield than it truly is.

The same loading conditions to the cavity are simulated with FEKO, and the good agreement with EIGER is observed in Figure 4. It is worth mentioning that the result for the 0 Ohm load has been truncated along the peak due to the limited frequency sampling in both the EIGER and FEKO response; theoretically, the value at resonance would continue to increase because of the absence of absorptive losses in both the cylinder and the long antenna. Practically, numerical leakage and physical leakage from the slot should limit the peak to a large, finite value. While in our frequency sweep EIGER estimates 30 dB at resonance for the 0 Ohm case, FEKO estimates about 12 dB.

As further illustration of the field-dampening effect, we plot the near field information computed with EIGER at the resonance peak of 49.02 MHz in Figure 5(b) along the red-dashed line close to the antenna shown in Figure 5(a). The large near-field variation is evident from the result in Figure 5(b).

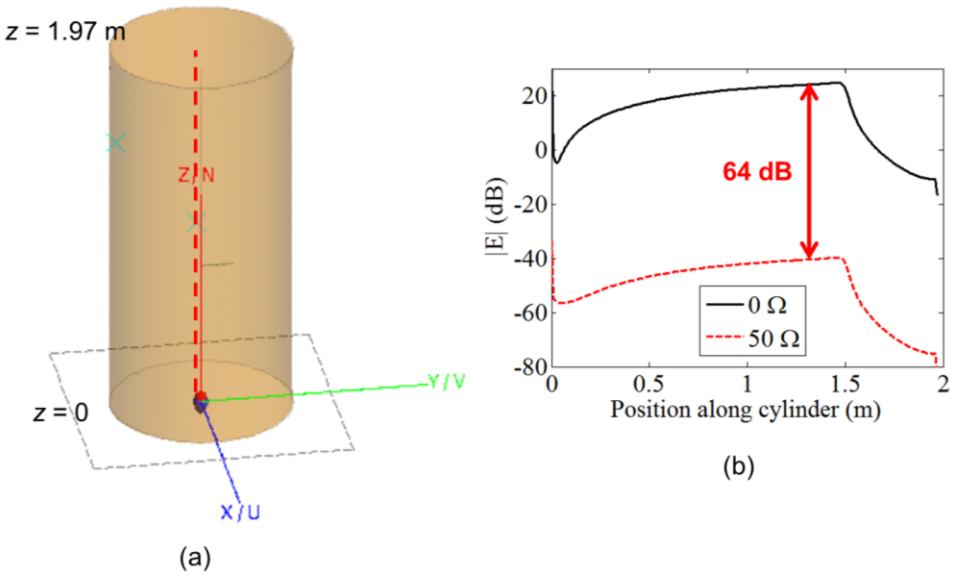

Figure 5. (a) Schematic of the cylinder with long antenna. The red-dashed line indicates the location of sampling points where the field is collected from EIGER simulations (shifted in the *y* direction by -0.0254 m). Magnitude of the near field versus axial position (z location, where *z* = 0 is located at the base of the cylinder) for the structure in panel (a).

We now include absorptive losses in the system: the cylinder is made of 6061 Al alloy with a conductivity of 2.6×10^7 S/m while the antenna is made of Cu with a conductivity of 5.8×10^7 S/m . In this case, we get a result similar to Figure 4, with the difference that now the peak result for the 0 Ohm load would be finite because of the presence of absorptive losses (see previous comments on Figure 4). While the results are not shown here, we still find a wide field

variation (greater than 60 dB) produced by the presence of the 50 Ohm load. This conclusion is also supported by FEKO simulations.

Thus far we have looked at the new mode generated by the antenna around 50 MHz; however, we next consider the effect of the antenna loading on the modes supported by the cavity. To answer this question, we take the case analyzed in Figure 4 without absorptive losses and perform a frequency sweep between 220 and 260 MHz with both loading conditions. The results using both EIGER and FEKO are shown in Figure 6. This range was chosen around the resonance frequency predicted by Eq. (1). The resonance corresponding to the *E* mode (0,1,0) is shifted to a lower frequency of approximately 240 MHz due to the presence of the long antenna (recall from Section 2 that the cavity without the antenna showed this mode around 251 MHz). The *H* mode (1,1,2) resonance is still present around 245 MHz and is unperturbed by the presence of the long antenna. One can observe a wide field variation (greater than 40 dB) produced by the presence of the 50 Ohm load when comparing the results for the two loading conditions. As described in previous results, the result for the 0 Ohm load has again been truncated due to limited frequency sampling points; the value at resonance would continue to increase because of the absence of any absorptive losses in the simulation. It is worth pointing out that, because the long wire antenna affects only the E_z field, the load in this case does not affect the *H* mode (1,1,2) resonant mode.

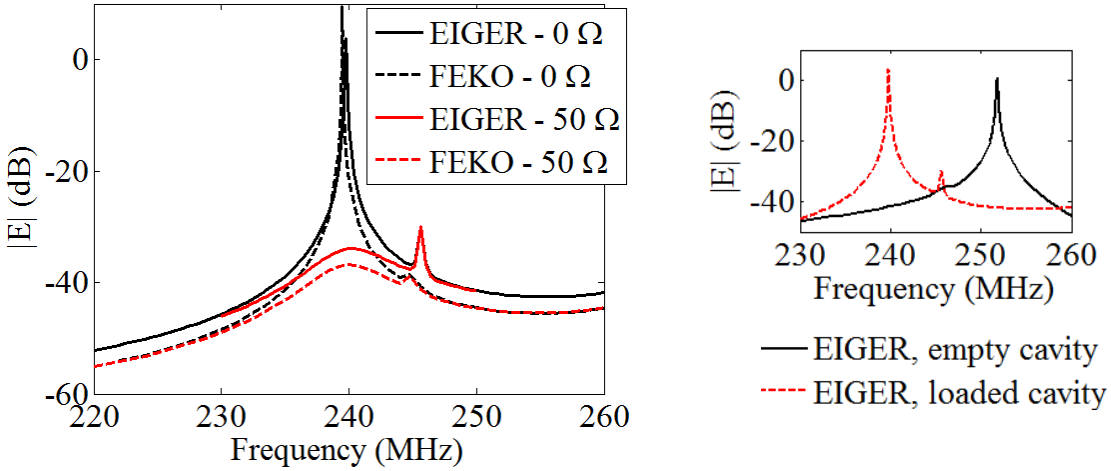

Figure 6. Frequency sweeps performed using EIGER and FEKO for the structure in Figure 1 containing a long wire antenna; this frequency band is located about the lowest order E mode resonance supported by the cylinder. The inset on the right shows a picture of the frequency shift between empty and loaded cavity with 0 Ohm load.

4. CONCLUSIONS

In this report we investigated the interior field response when a resonating cylindrical cavity containing a small perturbing slot (or aperture) is excited by an external electric field. We found that the interior cavity fields are significantly damped when a 50 Ohm terminated antenna is introduced into the system. In other words, the quality factor of the cavity is reduced when a long wire antenna (loaded) is used as the field "sensor". The lower quality factor (and dampening of field levels) results from the measurement instrumentation and disguises the field characteristics associated with the device-under-test (in this example, the slotted cylinder). If a long wire antenna is introduced into the cavity for measurements, an accurate characterization of the coupling will require that the antenna effects are extracted from the field measurements. If this is not done, the interior field levels will be underestimated and the shielding effectiveness of the cavity will appear much better than it is in actuality, particularly when is loaded by a 50 Ohm instrumentation. In order to accurately characterize the coupling into the cavity, a "non-perturbing" sensor (such as a monopole) is recommended. With this approach, the interior field distribution and peak levels characterizing the cavity will be fairly well preserved. It should be noted that to perform this same type of study for a large cavity structure at higher frequencies (and around higher-order interior cavity modes), numerical simulations will become increasingly time-intensive with frequency and most likely massively-parallel simulations will be required.

REFERENCES

[1] M. P. Robinson, T. M. Benson, C. Christopoulos, et al., "Analytical Formulation for the Shielding Effectiveness of Enclosures with Apertures," IEEE Transactions on Electromagnetic Compatibility 40(3), 240-248 (1998).
[2] X. C. Nie, N. Yuan, L. W. Li, and Y. B. Gan, "Accurate Modeling of Monopole Antennas in Shielded Enclosures with Apertures," Progress in Electromagnetics Research **79**, 251-262 (2008).
[3] E. S. Siah, K. Sertel, J. L. Volakis, V. V. Liepa, and R. Wiese, "Coupling Studies and Shielding Techniques for Electromagnetic Penetration Through Apertures on Complex Cavities and Vehicular Platforms," IEEE Transactions on Electromagnetic Compatibility **45**(2), 245-257 (2003).
[4] G. B. Tait, C. Hager, M. B. Slocum, and M. O. Hatfield, "On Measuring Shielding Effectiveness of Sparsely Moded Enclosures in a Reverberation Chamber", IEEE Transactions On Electromagnetic Compatibility **55**(2), 231-240 (2013).
[5] L. K. Warne, R. E. Jorgenson, J. T. Williams, L. I. Basilio, W. L. Langston, R. S. Coats, S. Campione, and K. C. Chen, "A Bound on Electromagnetic Penetration through a Slot Aperture with Backing Cavity," Sandia National Laboratories report SAND2016-9029, Albuquerque, NM, USA, 2016.
[6] D. R. Wilton, W. A. Johnson, R. E. Jorgenson, R. M. Sharpe, and J. B. Grant, "EIGER: A new generation of computational electromagnetics tools," retrieved from http://www.osti.gov/scitech/servlets/purl/219454 (1996).
[7] R. M. Sharpe, J. B. Grant, N. J. Champagne, W. A. Johnson, R. E. Jorgenson, D. R. Wilton, W. J. Brown, and J. W. Rockway, "EIGER: Electromagnetic Interactions GEneRalized," retrieved from http://www.osti.gov/scitech/servlets/purl/501495 (1997).
[8] EIGER, https://pulsedpower.sandia.gov/ppt_tech/compphys/Projects/eiger/eiger.html - 2017.
[9] FEKO, https://www.feko.info/ - 2017.
[10] CST Microwave Studio, https://www.cst.com/products/cstmws - 2017.
[11] M. B. Higgins and D. R. Charley, "Electromagnetic radiation (EMR) coupling to complex systems: Aperture coupling into canonical cavities in reverberant and anechoic environments and model validation," Sandia National Laboratories report SAND2007-7931, Albuquerque, NM, USA, 2007.
[12] H. G. Hudson, S. L. Stronach, W. Derr, W. A. Johnson, L. K. Warne, J. Kotulski, et al., "Cable test system upgrade coaxial cable/connector model validation experiments," Facility Test Report, Albuquerque, NM, 2001.

APPENDIX A

The axial fields satisfy the scalar Helmholtz equation

$$\left(\nabla^2 + k^2\right)\left(E_z, H_z\right) = 0 \tag{A1}$$

with $k^2 = \omega^2 \mu_0 \varepsilon_0$. We can thus take the solutions as

$$\left(E_z, H_z\right) = AJ_m\left(\varsigma\rho\right)\cos\left[m\left(\varphi - \varphi_0\right)\right]\left\{\cos\left(\alpha z\right), \sin\left(\alpha z\right)\right\} \quad 0 < \rho < a,\ 0 < z < h \tag{A2}$$

with $\varsigma = \sqrt{k^2 - \alpha^2}$ and φ_0 is arbitrary. Maxwell's equations when split into transverse and longitudinal field components are

$$\begin{aligned} \nabla \times \mathbf{E} &= \left(\nabla_t + \frac{\partial}{\partial z}\mathbf{e}_z\right) \times \left(\mathbf{E}_t + E_z \mathbf{e}_z\right) = i\omega\mu_0\left(\mathbf{H}_t + H_z \mathbf{e}_z\right) = i\omega\mu_0 \mathbf{H} \\ \nabla \times \mathbf{H} &= \left(\nabla_t + \frac{\partial}{\partial z}\mathbf{e}_z\right) \times \left(\mathbf{H}_t + H_z \mathbf{e}_z\right) = -i\omega\varepsilon_0\left(\mathbf{E}_t + E_z \mathbf{e}_z\right) = -i\omega\varepsilon_0 \mathbf{E} \end{aligned} \tag{A3}$$

***H* modes:**

For *H* modes, these yield

$$\begin{aligned} &\mathbf{e}_z \times \frac{\partial}{\partial z}\mathbf{E}_t = i\omega\mu_0 \mathbf{H}_t \\ &\nabla_t \times \mathbf{E}_t = i\omega\mu_0 H_z \mathbf{e}_z \\ &\nabla_t \times \left(H_z \mathbf{e}_z\right) + \mathbf{e}_z \times \frac{\partial}{\partial z}\mathbf{H}_t = \mathbf{e}_z \times \left(\frac{\partial}{\partial z}\mathbf{H}_t - \nabla_t H_z\right) = -i\omega\varepsilon_0 \mathbf{E}_t \\ &\nabla_t \times \mathbf{H}_t = 0 \end{aligned} \tag{A4}$$

From the first equation in (A4)

$$\mathbf{e}_z \times \frac{\partial^2}{\partial z^2}\mathbf{E}_t = -\alpha^2 \mathbf{e}_z \times \mathbf{E}_t = i\omega\mu_0 \frac{\partial}{\partial z} H_z \tag{A5}$$

and thus from the third equation in (A4)

$$-i\omega\mu_0 \mathbf{e}_z \times \nabla_t H_z = \left(k^2 - \alpha^2\right)\mathbf{E}_t \tag{A6}$$

and using the first equation in (A4)

$$\frac{\partial}{\partial z}\nabla_t H_z = \left(k^2 - \alpha^2\right)\mathbf{H}_t \tag{A7}$$

For the *H* modes (H_z) the axial field must vanish on the ends

$$H_z\left(z = 0, h\right) = 0 \rightarrow \sin\left(\alpha h\right) = 0 \tag{A8}$$

so we must take the sine function with $\alpha = \alpha_n = n\pi / h$, $n = 1,2,\ldots$. Then, the vanishing of the E_φ on the side wall means that

$$\frac{\partial H_z}{\partial \rho}(\rho = a) = 0 \to J_m'\left(j_{m,p}'\right) = 0 \tag{A9}$$

so we must take (note that 0 is also a trivial root of the $m = 0$ Bessel function)

$$\begin{aligned}
&\varsigma = \varsigma_{m,p} = j_{m,p}'/a \quad p = 1,2,\ldots \\
&j_{0,p}' = 3.83171, 7.01559, \ldots \\
&j_{1,p}' = 1.84118, 5.33144, 8.53632, \ldots \\
&j_{2,p}' = 3.05424, 6.70613, 9.96947, \ldots \\
&j_{3,p}' = 4.20119, 8.01524, \ldots \\
&j_{4,p}' = 5.31755, 9.28240, \ldots
\end{aligned} \tag{A10}$$

and

$$H_z = AJ_m\left(j_{m,p}'\rho/a\right)\cos\left[m(\varphi - \varphi_0)\right]\sin\left(n\pi z/h\right) \quad 0 < \rho < a,\ 0 < z < h \tag{A11}$$

The resonant frequencies are thus given by

$$k_{m,p,n} = \omega_{m,p,n}\sqrt{\mu_0\varepsilon_0} = \sqrt{\varsigma_{m,p}^2 + \alpha_n^2} = \sqrt{\left(j_{m,p}'/a\right)^2 + \left(n\pi/h\right)^2} \tag{A12}$$

***E* modes:**

For *E* modes (E_z) Maxwell's equations yield

$$\begin{aligned}
&\nabla_t \times \left(E_z \mathbf{e}_z\right) + \mathbf{e}_z \times \frac{\partial}{\partial z}\mathbf{E}_t = i\omega\mu_0 \mathbf{H}_t \\
&\nabla_t \times \mathbf{E}_t = 0 \\
&\mathbf{e}_z \times \frac{\partial}{\partial z}\mathbf{H}_t = -i\omega\varepsilon_0 \mathbf{E}_t \\
&\nabla_t \times \mathbf{H}_t = -i\omega\varepsilon_0 E_z \mathbf{e}_z
\end{aligned} \tag{A13}$$

From the third equation in (A13)

$$\mathbf{e}_z \times \frac{\partial^2}{\partial z^2}\mathbf{H}_t = -\alpha^2 \mathbf{e}_z \times \mathbf{H}_t = -i\omega\varepsilon_0 \frac{\partial}{\partial z}\mathbf{E}_t \tag{A14}$$

and thus from the first equation in (A13)

$$i\omega\varepsilon_0 \mathbf{e}_z \times \nabla_t E_z = \left(k^2 - \alpha^2\right)\mathbf{H}_t \tag{A15}$$

and using the third equation in (A13)

$$\frac{\partial}{\partial z}\nabla_t E_z = \left(k^2 - \alpha^2\right)\mathbf{E}_t \tag{A16}$$

For the *E* modes (E_z) the axial field must vanish on the cylindrical wall

$$E_z(\rho = a) = 0 \to J_m\left(j_{m,p}\right) = 0 \tag{A17}$$

so we must take

$$\begin{aligned}
&\varsigma = \varsigma_{m,p} = j_{m,p}/a \quad p = 1,2,\ldots \\
&j_{0,p} = 2.40482, 5.52008, 8.65372, \ldots \\
&j_{1,p} = 3.83171, 7.01559, 10.17347, \ldots \\
&j_{2,p} = 5.13562, 8.41724, \ldots \\
&j_{3,p} = 6.38016, 9.76102, \ldots \\
&j_{4,p} = 7.58834, 11.06471, \ldots
\end{aligned} \tag{A18}$$

Then the vanishing of the tangential electric field on the ends

$$\frac{\partial E_z}{\partial \rho}(z = 0, h) = 0 \to \sin(\alpha h) = 0 \tag{A19}$$

means that we must choose the cosine and set $\alpha = \alpha_n = n\pi/h$, $n = 0,1,2,\ldots$. Thus

$$E_z = AJ_m\left(j_{m,p}\rho/a\right)\cos\left[m(\varphi - \varphi_0)\right]\cos(n\pi z/h) \quad 0 < \rho < a,\ 0 < z < h \tag{A20}$$

The resonant frequencies are thus given by

$$k_{m,p,n} = \omega_{m,p,n}\sqrt{\mu_0\varepsilon_0} = \sqrt{\varsigma_{m,p}^2 + \alpha_n^2} = \sqrt{\left(j_{m,p}/a\right)^2 + (n\pi/h)^2} \tag{A21}$$

DISTRIBUTION

Number	Mail Stop	Name	Dept.
1 (electronic)	MS0899	Technical Library	9536
1 (electronic)	MS1152	R. E. Jorgenson	1352
1 (electronic)	MS1152	L. I. Basilio	1352
1 (electronic)	MS1152	S. Campione	1352
1 (electronic)	MS1152	L. K. Warne	1352
1 (electronic)	MS1152	R. S. Coats	1352
1 (electronic)	MS1152	K. Sainath	1352
1 (electronic)	MS1152	S. F. Glover	1353
1 (electronic)	MS1152	M. A. Dinallo	1354
3	MS1152	L. K. Warne	1352
3	MS1152	S. Campione	1352
3	MS1152	L. I. Basilio	1352
1 (electronic)	MS1168	L. X. Schneider	1350


Sandia National Laboratories